THE DYNAMICAL PROCESS OF A CORONAL TRANSIENT ASSOCIATED WITH AN ERUPTIVE PROMINENCE

I. *Basic Mechanism*

WEN-RUI HU

Institute of Mechanics, Academia Sinica, Beijing, China

(Received 5 January, 1983)

Abstract. The statistical correlation between an eruptive prominence and the coronal transient associated with this prominence implies that there should be a relationship between these two kinds of dynamical processes. This paper analyzes the dynamical effect of a plasma 'piston' in the corona, consisting of an eruptive prominence and/or a magnetic flux region (loop or arcade, or blob) in front of the prominence. Ahead of the piston, there is a compressed flow, which produces a shock front. This high-density region corresponds to the bright feature of the transient. Behind the piston, there is a rarefaction region, which corresponds to the dark feature of the transient. Therefore, both the bright and dark features of the transient may be explained at the same time by the dynamical process of the moving piston.

Two local solutions, one perpendicular and one parallel to the direction of solar gravitational field, are discussed. The influence of gravity on the gas-dynamical process driven by the piston is discussed in terms of characteristic theory, and the flow field is given quantitatively. For a typical piston trajectory similar to the one for an eruptive prominence, the velocity of the shock front which locates ahead the transient front is nearly constant or slightly accelerated, and the width of the compressed flow region may be kept nearly constant or increased linearly, depending on the velocity distribution of the piston. Based on these results, the major features of the transient may be explained. Some of the fine structure of the transient is also shown, which may be compared in detail with observations.

1. Introduction

The coronal transient is an important phenomenon of solar activity in the corona. It was first observed in the coronal measurements of the white-light coronagraph aboard Skylab and OSO-7 (MacQueen *et al.*, 1974; Howard *et al.*, 1976) and more recently aboard the Solar Maximum Mission satellite (Chipman, 1981). These observations have shown that the dense plasma corresponding to the observed bright feature of a transient propagates outward with nearly constant (or slightly accelerating) velocity in the typical time of tens of minutes, and that transients are correlated statistically with eruptive prominences and flares (Munro *et al.*, 1979). During the past few years, observations made with a ground-based coronameter have supplied information on the initial process in the lower corona (Fisher and Poland, 1981; Fisher *et al.*, 1981), showing that the transient associated with an eruptive prominence begins as a depletion in the corona which corresponds to the observed dark features. The observed morphologies of coronal transients vary widely; some of them appear as loops or arcades, others as clouds or blobs (MacQueen, 1980).

Many physical mechanisms have been suggested (see, for example, the review of Rust

Astrophysics and Space Science **92** (1983) 373–394. 0004–640X/83/0922–0373$03.30.
Copyright © 1983 by D. Reidel Publishing Co., Dordrecht, Holland, and Boston, U.S.A.

et al., 1979). The basic approaches may be classified into three kinds: numerical experiments, local analysis, and special solutions applied to explain the transient process.

The numerical approach assumed that there exists pulsed increment of a thermodynamic parameter (pressure or density, or temperature) or an increment of the magnetic field in a local region, which may be associated with some energy release, e.g., from a solar flare. As a result of the non-equilibrium of the initial condition, the coronal plasma is driven outward and a shock-wave front forms easily. The bright feature of the transient may be explained by the density increment behind the shock front (Nakagawa *et al.*, 1975, 1978; Steinolfson and Nakagawa, 1977; Wu *et al.*, 1978; Dryer *et al.*, 1979). The advantage of the numerical computations is that they can show the evolution of the two-dimensional configuration. However, the computational results depend on many conditions which must be assumed in computation.

Those who employ local analysis confined their interest to the local region near the top of the configuration. Therefore, the problem reduces to one dimension and time dependent. Anzer (1978) discussed a loop-like magnetic flux tube with two feet fixed at its base, driven by the Lorentz force. Mouschovias and Poland (1978) suggested a twisted magnetic field tube driven outward by the magnetic pressure gradient. Pneuman (1980) analyzed the transient processes associated with an eruptive prominence, and determined that the propagation velocity approached constancy at large distances and that the width of the loop or arcade increased linearly with the time and distance; both results fit observations qualitatively. Recently, Yeh and Dryer (1981) pointed out the influence of plasma pressure on the moving process of a transient loop, and suggested that the transient is driven by the magnetohydrodynamic buoyancy force. Because of its simplicity, local analysis may give a very clear physical picture of the propagating process of the transient. However, all the models consider that the magnetic force is the major driving force; thus a local approach must assume some configuration of an evolving magnetic field.

Recently, Low *et al.* (1982) considered a two-dimensional model of a magnetic field emerging into the corona, and compared their results with the observations of the depletion feature in the initial process of the transient. However, the propagating process is not very clear, as the velocity field is difficult to discuss. An unsteady two-dimensional similarity solution was applied to the transient process (Low, 1982), as a first step toward analyzing the evolution of the complete two-dimensional processes between the magnetic field and the moving plasma. Because the solution is a special one, however, the relationship between this special mathematical solution and the observed physical process of coronal transient is not very clear.

The purpose of the present paper is to discuss the influence of an eruptive prominence on the transient process. If we consider a magnetic flux tube propagating in a medium of compressible plasma, there are gasdynamical processes on both sides of the flux tube, similar to those of a moving piston. Here, we must include the gravity of the Sun. Stanyukovich (1960) discussed some special solution for the unsteady motion of a gas in a gravitational field, for example, by assuming constant gravity or a polytropic index $\gamma = 3$. The characteristic relationships of one-dimensional unsteady flow with gravitation

were discussed by Thompson (1972) and Nakagawa and Steinolfson (1976). We will apply characteristic theory to analyze the transient process.

2. Physical Picture

Statistical analysis shows that over 70% of coronal transients are associated with an eruptive prominence (Munro *et al.*, 1979). Eruptive prominences occur mainly in the lower levels of the solar atmosphere, and transients propagate into the outer corona. Pneuman (1980) discussed the relationship between these active phenomena in detail, and suggested that the mechanism which precipitates the prominence eruption also produces the transient. In this paper, we consider the influence of the eruptive prominence on the transient process. It seems that the prominence eruption may be a driving mechanism, compressing the plasma ahead of it and producing a depletion region behind it. The compressed plasma corresponds to the region of observed high density and appears as a bright loop or cloud in white light. On the other hand, the depletion region in the lower corona manifests itself as the dark feature of the transient.

From the point of view of energy, the energy of a large eruptive prominence may be sufficient to supply a transient. For example, if we adopt an eruptive velocity of $v_{ep} = 400$ km s^{-1}, the density of the prominence is $\rho_{ep} = 5 \times 10^{10}$ cm^{-3} and the typical volume of the prominence is $V_p = (10^{10}\text{ cm}) \times (5 \times 10^9\text{ cm}) \times (2 \times 10^8\text{ cm})$ (see, for example, Allen, 1973; Tandberg-Hanssen, 1974). Thus, the kinetic energy of this eruptive prominence is roughly

$$\rho_{ep} v_{ep}^2 V_p \approx 10^{30}\text{ ergs}\,. \tag{2.1}$$

The kinetic energy estimated in (2.1) is only a typical value; it may have a deviation of one to two orders of magnitude. However, the typical energy of a transient associated with an eruptive prominence is (see MacQueen, 1980)

$$E_t \approx 0.9 \times 10^{30}\text{ ergs}\,. \tag{2.2}$$

Therefore, the energy of both the eruptive prominence and the transient associated with it may have the same order of magnitude. If the kinetic energy of the eruptive prominence is smaller than that of the transient, the plasma pressure of Lorentz force will drive the transient. In this case, the dynamical effect, locally, of the motion driven by this force is similar to that of the eruptive prominence, if the magnetic field is frozen with the plasma in the local region. Consequently, we will analyze the dynamical effect for a moving 'piston' of plasma, which may be an eruptive prominence, a magnetic flux region or tube, or both. The dynamical process of this plasma piston in the corona is similar to the gasdynamic process of a piston moving in a shock tube (see Dryer, 1981; Maxwell and Dryer, 1981).

The velocity profiles of an eruptive prominence and its associated transient are given typically from observations as in Figure 1 where the solid line is the trajectory of the eruptive prominence and the broken line is the trajectory of the associated transient. The morphology of the evolutionary process for the transient is described schematically in

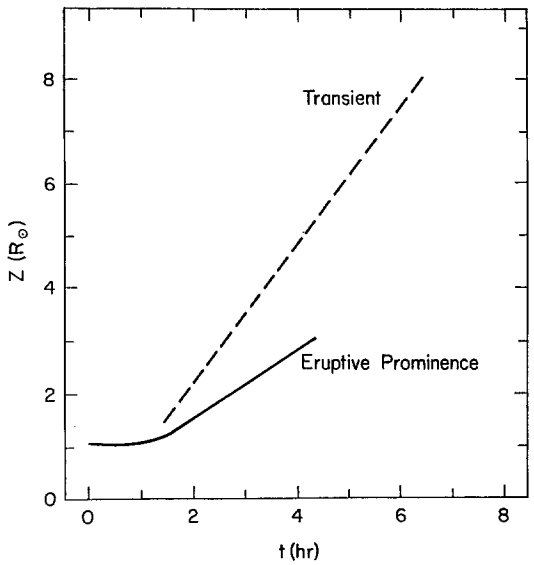

Fig. 1. Typical observed profiles of an eruptive prominence and a transient associated with eruptive prominence.

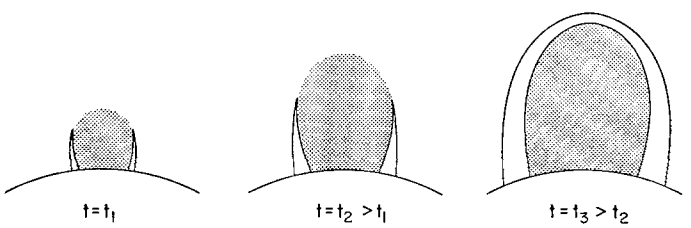

Fig. 2. The evolutionary morphology of a transient associated with an eruptive prominence.

Figure 2 (Low *et al.*, 1982). Combining the results from both figures, we may surmise that as the prominence moves along its trajectory (solid line in Figure 1) a rarefaction flow propagates backward in the region to the left of the trajectory. This region corresponds to a depletion of density and manifests itself as the dark feature of the transient in Figure 2. In the classical problem of a plane piston, there is a compressed region ahead of the piston with uniform flow parameters, forming a shock front where it contacts the quiet region. But, because of the influence of gravity, the parameters in the compressed region will change with time and distance. Therefore, a high-density region will propagate outwards ahead of the depletion region, and will be manifested as the bright feature of the transient as shown in Figure 2. The dynamical processes produce these regions of density increase and density depletion at the same time, and may be applied to explain the major features of the transient processes.

3. Mathematical Description

In principle, the transient process has a configuration of at least two dimensions. So, it should be described as an unsteady two-dimensional flow, as in the approaches that use either numerical experimentation (Wu *et al.*, 1978; Dryer *et al.*, 1979) or some special solution (Low, 1982). However, the local analysis method could clearly shed light on the mechanism of the dynamical process and the essential physical picture. We will first discuss the flow features in the regions near the top and the base of the configuration, respectively, then show the two-dimensional evolution of the transient.

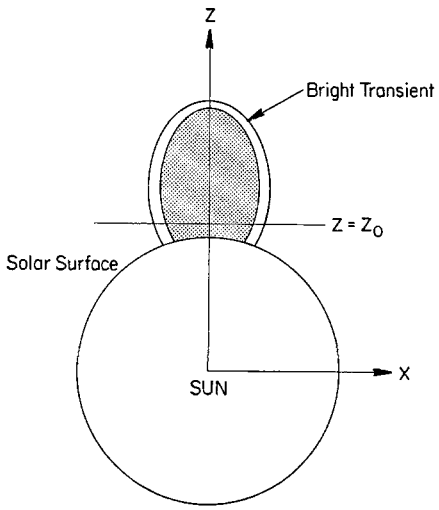

Fig. 3. The coordinate system dopted in the text.

We use the Cartesian coordinate x, y, z, whose origin is at the center of Sun and whose z axis intersects the top of transient, as shown in Figure 3. Some symmetry is assumed here. The gasdynamical equations near the z axis may be written as

$$\frac{\partial \rho}{\partial t} + \frac{\partial \rho w}{\partial z} = 0 , \tag{3.1}$$

$$\rho \left(\frac{\partial w}{\partial t} + w \frac{\partial w}{\partial z} \right) = - \frac{\partial p}{\partial z} - \rho \frac{GM}{z^2} , \tag{3.2}$$

$$\frac{\partial}{\partial t} \left(\frac{p}{\rho^\gamma} \right) + w \frac{\partial}{\partial z} \left(\frac{p}{\rho^\gamma} \right) = 0 , \tag{3.3}$$

where p and ρ are plasma pressure and density, respectively, w is the velocity component in the z direction, M is the mass of Sun, and G is the gravitational constant.

The equations at level $z = z_0$ (near base), where the z component of the velocity is zero, may be written as

$$\frac{\partial \rho}{\partial t} + \frac{\partial \rho u}{\partial x} = 0 , \tag{3.4}$$

$$\rho \left(\frac{\partial u}{\partial t} + u \frac{\partial u}{\partial x} \right) = - \frac{\partial p}{\partial x} , \tag{3.5}$$

$$\frac{\partial}{\partial t} \left(\frac{p}{\rho^\gamma} \right) + u \frac{\partial}{\partial x} \left(\frac{p}{\rho^\gamma} \right) = 0 , \tag{3.6}$$

where u is the velocity component in the direction of the x axis. In above equations, the solar gravity is not important when we consider motion parallel to the solar surface. The difference between Equations (3.1)–(3.2) and (3.4)–(3.6) is that the influence of solar gravity is present near the top region and absent near the base region. It is clear, then, that the flow field near the base may be discussed approximately in terms of pure gasdynamics without gravity, which has been studied extensively (see, for example, Landau and Lifshitz, 1959). We use this idea to discuss the solution near the base level, and then the region near the top.

4. Dynamical Features Near the Base

Observations show that the transient expands to both sides at the base of the lower corona. Figure 4 gives one set of observed results along, the baselength, denoted as square marks (Low *et al.*, 1982). The trajectory at the top of the transient is denoted as circles in the same figure. It may be imagined that the expansive velocity of the bright front at $z = z_0$ is nearly constant, as shown by the broken line in Figure 4.

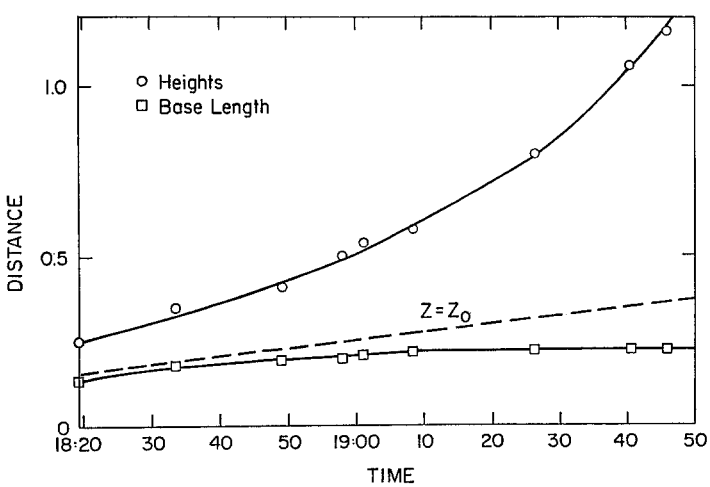

Fig. 4. Trajectories of a transient at the top and the base length on 5 August, 1980.

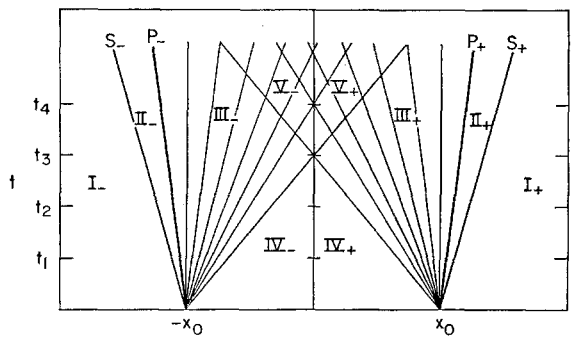

Fig. 5. Flow regions of the transient near the base level.

The flow characteristics are given in Figure 5. Here, the lines x_0P_+ and $-x_0P_-$ are the trajectories of pistons corresponding to the two legs of the transient at $z = z_0$, and x_0S_+ and $-x_0S_-$ are the fronts of shock waves. There are two flow regions II_+ and II_-, respectively, in front of the pistons on each side. The flow parameters in region I_+ or I_- are given by the conditions in the quiet corona (ignoring, for simplicity, the background solar wind): that is

$$v_I = 0\,, \qquad p_I = p_{\text{quiet corona}}\,, \qquad \rho_I = \rho_{\text{quiet corona}}\,,$$

where the values of the quiet corona are taken at level $z = z_0$. According to the gasdynamic theory of the piston, the flow field can be determined completely if the parameters at the position of the moving piston and in the quiet region are both given. For example, if the piston velocity v_p is constant, the velocity of the shock front may be given as

$$v_s = \frac{\gamma + 1}{4}\, v_p + \left[a_1^2 + \left(\frac{\gamma + 1}{4} \right)^2 v_p^2 \right]^{1/2}; \tag{4.1}$$

and the solutions in region II are:

$$v_{II} = v_p\,, \tag{4.2}$$

$$p_{II} = p_I + \frac{2\rho_I}{\gamma + 1}\, [(v_s - v_p)^2 - a_1^2]\,, \tag{4.3}$$

$$\rho_{II} = \rho_I \frac{1}{\dfrac{\gamma - 1}{\gamma + 1} + \dfrac{2}{\gamma + 1} \left(\dfrac{a_I}{v_s - v_p} \right)^2}\,, \tag{4.4}$$

where the subscription II corresponds to both regions II_+ and II_-. Obviously, the density in region II is larger than the density in region I.

Behind the moving piston, there are three regions III_+, IV_+, and V_+ or III_-, IV_-, and V_-; the boundary between regions III and IV is a characteristic line. The parameters

in region IV are given by the condition of quiet prominence behind the eruptive prominence, which may be different from the condition in region I. The flow in region III may be considered as Riemann flow, and the solution in region III may be obtained as

$$|v_{\mathrm{III}}| = \frac{2}{\gamma+1}\left|\frac{x}{t} - a_{\mathrm{IV}}\right|, \tag{4.5}$$

$$\rho_{\mathrm{III}} = \rho_{\mathrm{IV}}\left(1 - \frac{\gamma-1}{2}\frac{|v_{\mathrm{III}}|}{a_{\mathrm{IV}}}\right)^{2/(\gamma-1)}, \tag{4.6}$$

$$p_{\mathrm{III}} = p_{\mathrm{IV}}\left(1 - \frac{\gamma-1}{2}\frac{|v_{\mathrm{III}}|}{a_{\mathrm{IV}}}\right)^{2\gamma/(\gamma-1)}. \tag{4.7}$$

Relation (4.6) shows that the density distributions in regions III_+ and III_- obey the principles of rarefaction flow and correspond to the depletion process. If the velocity of the piston is large enough, there may be a region with uniform parameters between regions III and II behind the moving piston (as discussed in the gasdynamics).

The rarefaction flows produced by piston P_+ and P_-, respectively, will come into collision after time t_3, as shown in Figure 5.

According to the above discussions, the evolution of the density distribution produced by a pair of moving pistons in the lower corona may be shown in Figure 6. Ahead of the pistons is the compressed region II, which corresponds to the bright feature of transient propagating into both sides near the base. The width of the bright region II

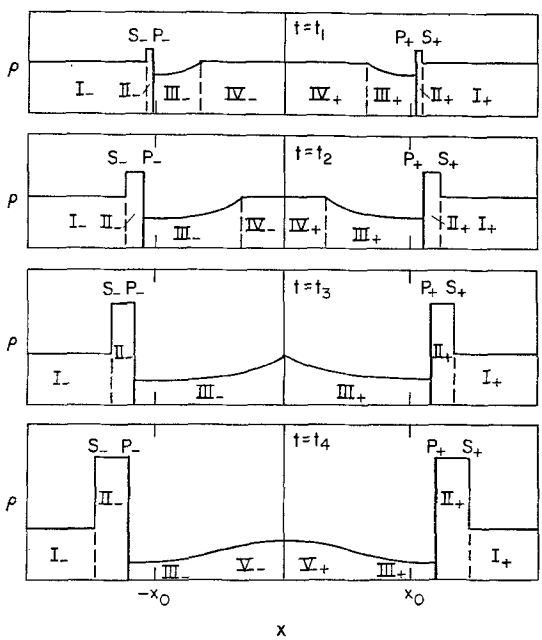

Fig. 6. The evolution of the density profile at the level $z = z_0$.

increases linearly with time if the piston velocity is constant; the faster the piston velocity, the narrower the compressed region. Behind the piston is a rarefaction flow propagating toward the plane $x = 0$, with the sonic velocity a_{IV}. The depletion density region between the piston and the quiet corona region IV will grow gradually. All these features agree qualitatively with the observations.

5. Dynamical Features Near the Top

Now we discuss the flow features in the local region near the top. The gravity of the Sun has an important influence on the flow near the top because its order of magnitude is larger. According to the theory of dimensional analysis, there are two typical velocities, that is,

$$\frac{z}{t} \quad \text{and} \quad \frac{\sqrt{GM}}{z} .$$

Therefore, the Riemann flow and Riemann invariants do not exist in general, but there are some special similarity solutions (see, for example, the gasdynamical solution by Sedov, 1959; Stanyukovich, 1960; and the MHD solution by Low, 1982). On the basis of discussions in the last section, it seems that these special similarity solutions can be applied to certain flow regions of the transient process, but it is difficult to describe the complete process. Local analysis although simplified, is better for understanding the physical mechanism.

The relationship between the eruptive prominence and the transient associated with it shows schematically in Figure 7. The eruptive prominence initially has a small velocity and then accelerates while the velocity of the transient is compressed by the accelerated piston, a strong shock wave will form ahead of the piston. This process may be analyzed

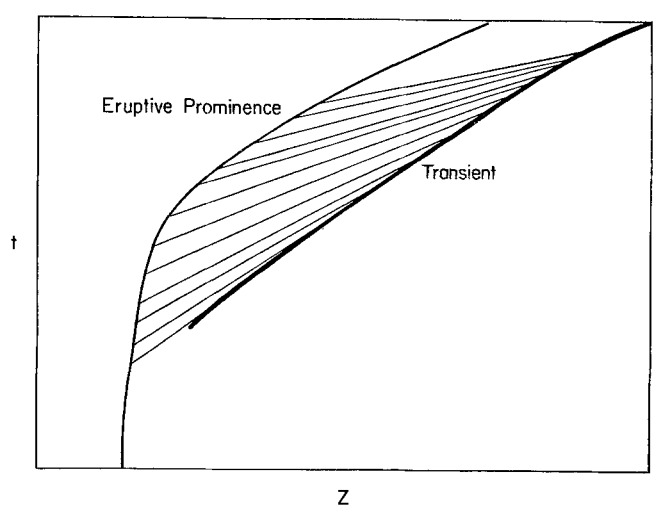

Fig. 7. Relationship between an eruptive prominence and a transient associated with it.

by the characteristic theory of hyperbolic equations. The hyperbolic Equations (3.1)–(3.3) have three characteristic lines. These lines and the relationships among them may be expressed as (see Appendix I)

$$\frac{\mathrm{d}z}{\mathrm{d}t} = w + a\,, \tag{5.1}$$

$$\mathrm{d}w + \frac{2}{\gamma - 1}\,\mathrm{d}a = -\frac{GM}{z^2}\,\mathrm{d}z\,; \tag{5.2}$$

$$\frac{\mathrm{d}z}{\mathrm{d}t} = w - a\,, \tag{5.3}$$

$$\mathrm{d}w - \frac{2}{\gamma - 1}\,\mathrm{d}a = -\frac{GM}{z^2}\,\mathrm{d}z\,; \tag{5.4}$$

$$\frac{\mathrm{d}z}{\mathrm{d}t} = 0\,, \tag{5.5}$$

$$\mathrm{d}(p/\rho^{\gamma}) = 0\,; \tag{5.6}$$

where isotropy is assumed in (5.2) and (5.4).

Consider a special characteristic line where the velocity is zero along it. In this case, (5.1)–(5.4) may then be written as

$$\frac{\mathrm{d}z}{\mathrm{d}t} = \pm a\,, \tag{5.7}$$

$$\frac{2}{\gamma - 1}\,\mathrm{d}a = \mp\frac{GM}{z^2}\,\mathrm{d}t\,. \tag{5.8}$$

From the above relations we have

$$\frac{2}{\gamma - 1}\,a\,\mathrm{d}a = -\frac{GM}{z^2}\,\mathrm{d}z\,, \tag{5.9}$$

or

$$\frac{a^2}{\gamma - 1} - \frac{GM}{z} = \text{const.} \tag{5.10}$$

On the other hand, the momentum equation (3.2) gives the condition of static equilibrium as

$$\frac{\partial p}{\partial z} = -\rho\,\frac{GM}{z^2}\,. \tag{5.11}$$

This may be rewritten as

$$\frac{2a}{\gamma-1}\frac{\partial a}{\partial z}-\frac{a^2}{\gamma-1}\frac{\partial \ln s}{\partial z}=-\frac{GM}{z^2}\,. \tag{5.12}$$

Equation (5.9) is the same as (5.12) in the case of an isotropic fluid. Therefore, the characteristic line (5.1) and (5.2) may be the boundaries between the flow region and the quiet corona.

Now we discuss the flow feature. If we introduce the non-dimensional parameters

$$w^*=\frac{w}{\sqrt{\frac{GM}{z_0^2}}}\,,\qquad a^*=\frac{a}{\sqrt{\frac{GM}{z_0^2}}}\,,\qquad z^*=\frac{z}{z_0}\,,\qquad t^*=\frac{t}{\sqrt{z_0^3/GM}}\,. \tag{5.13}$$

where z_0 is the solar radius, then the characteristic lines and relationships are

$$\frac{\mathrm{d}z^*}{\mathrm{d}t^*}=w^*\pm a^* \tag{5.14}$$

$$\mathrm{d}w^*\pm\frac{2}{\gamma-1}\,\mathrm{d}a^*=-\frac{\mathrm{d}t^*}{z^{*2}}\,. \tag{5.15}$$

The gravity term in the right-hand side of Equation (5.15) is positive for $\mathrm{d}t^*<0$, and negative for $\mathrm{d}t^*>0$. If the velocity does not change greatly, the local sonic velocity, and hence the temperature, will decrease along line (5.1) and increase along line (5.3) as $\mathrm{d}t^*>0$. The former may apply to the compressible flow and the latter to the rarefaction flow. In general, the velocity will also change along the characteristic lines. Similar to the cases of usual gasdynamics, there exist three typical flows by the break-up of an initial discontinuity: two shock waves propagating in opposite directions; one shock

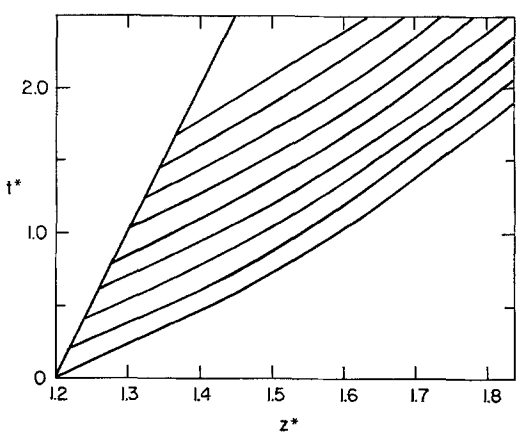

Fig. 8. Characteristic lines in the compressed region for the case including solar gravity, when the piston velocity is constant.

wave and one rarefaction wave propagating on each side, respectively; and two rarefaction wave propagating on both sides, with or without a vacuum region between the two wave fronts (see, for example, Landau and Lifshitz, 1959). However, the profiles of the parameters in the case including gravity are different from those in the case without gravity.

For a typical piston problem in gravity, the characteristic line and flow field may be determined by the characteristic method (see Appendix II), if the conditions at the piston are given. For example, Figures 8, 9, and 10 give the characteristic line of (5.1),

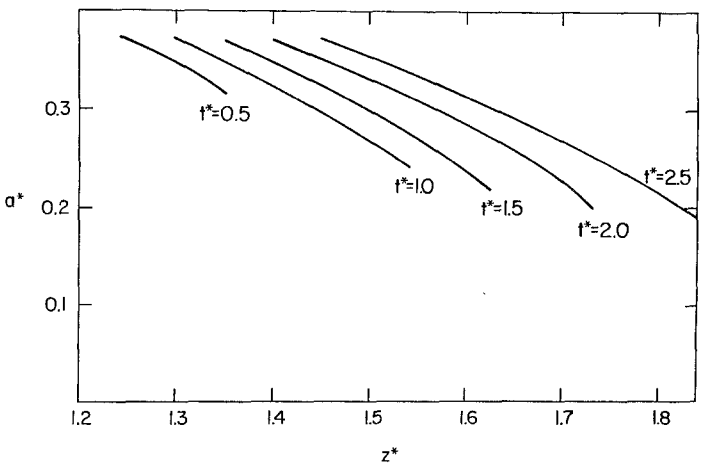

Fig. 9. Profile of the sonic velocity in the compressed region.

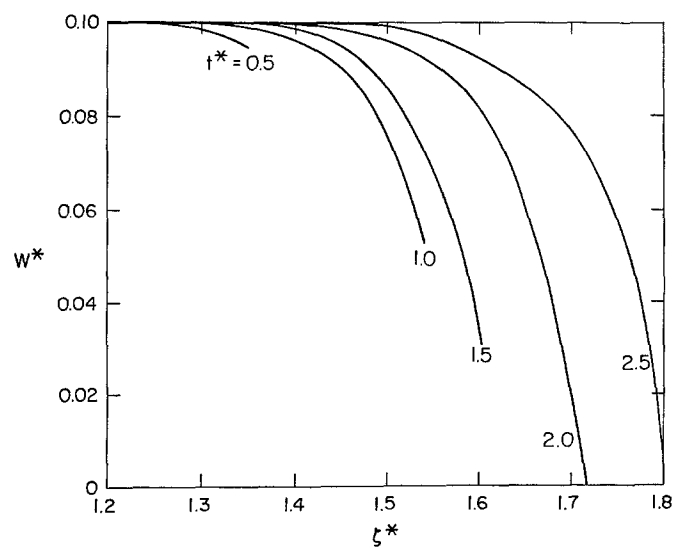

Fig. 10. Profile of the plasma velocity in the compressed region.

the distribution of the sonic velocity, and the plasma velocity, respectively, where the sonic and plasma velocities at the moving piston are taken as constant: i.e.,

$$w_p^* = 0.1\,, \qquad a_p^* = 0.375\,. \tag{5.13}$$

This case corresponds to the starting process of an eruptive prominence and the compressed flow produced by it. Similarly, the parameters of rarefaction flow are given in Figures 11, 12, and 13, respectively, for the same conditions at the piston as given by (5.13).

These figures show clearly the influence of solar gravity on the characteristic lines and relations. For the compressed flow, the characteristic line (5.1) is nearly linear but a bit curved, as shown in Figure 8, and both the sonic velocity and the plasma velocity decrease in the propagating process, as shown in Figures 9 and 10, respectively. In the case without gravity, the parameters remain constant. As the plasma velocity decreases

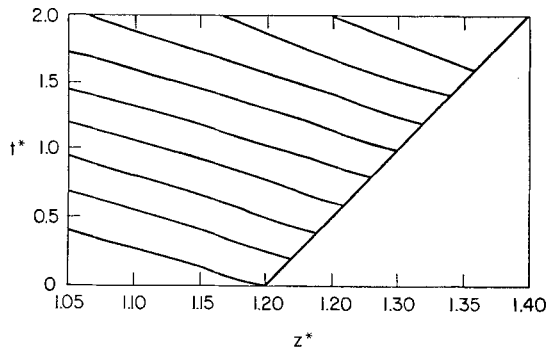

Fig. 11.

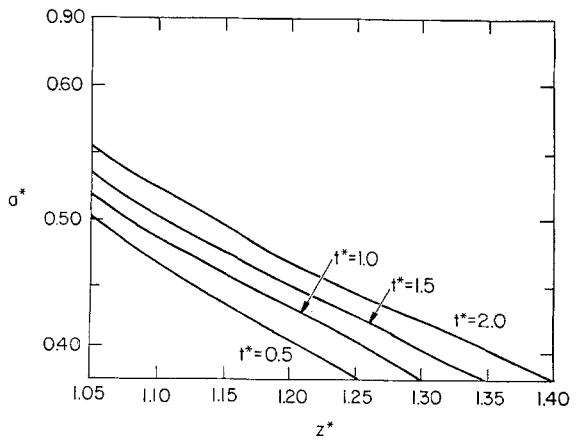

Fig. 12. Characteristic lines in the rarefaction region for the case including solar gravity, when the piston velocity is constant.

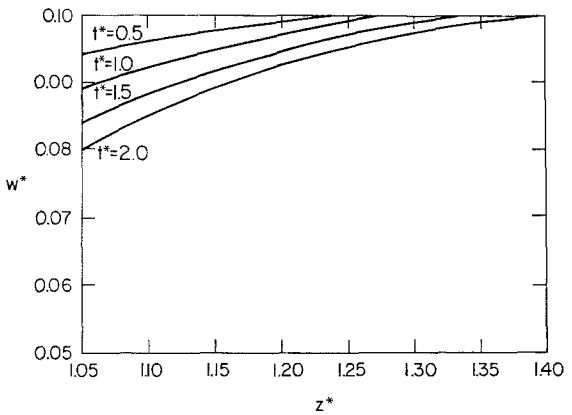

Fig. 13. Profiles of the plasma velocity in the rarefaction region.

to zero, the interface of the quiet corona and the compressed flow may sometimes be a weak discontinuous surface instead of a shock wave. In general, if the interface is a shock front, the strength of the shock wave will be weaker compared to the one without gravity, because of the decreasing velocity. In the case of the rarefaction flow, the sonic velocity increases, as shown in Figure 12, and the plasma velocity decreases as the fluid flows downward. The basic features of the rarefaction flow here are similar to those in the case without gravity; however, the quantitative relations are changed.

From the above discussions, it can be seen that the basic flow features with the influence of gravity included are similar to those for the case without gravity as given in Figures 5 and 6 in the last section. Observations show that the velocity of a prominence, and thus the piston of moving plasma, is not constant, as given in Figure 1. It is nearly constant at the initial period and then increases. According to gasdynamic theory, the characteristic lines will converge and then cross each other to form a shock front, which is manifested as the bright features of the forward part of the transient. For

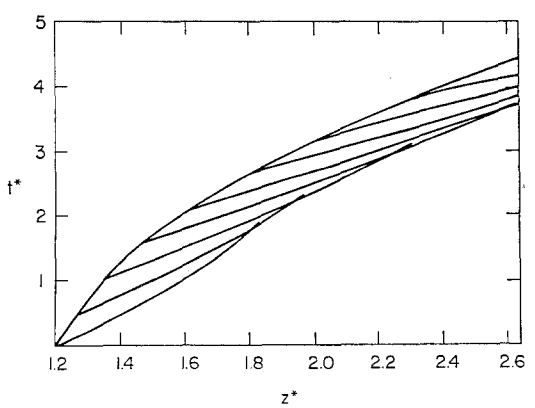

Fig. 14. Characteristic lines in the compressed region for the case including solar gravity, when the piston accelerates. The shock forms at the point where the line cross.

quantitative discussion, we assume a piston velocity

$$v_p^* = 0.1 + 0.1t^* , \tag{5.14}$$

$$a_p^* = 0.375 . \tag{5.15}$$

The distribution of characteristic lines is given in Figure 14, which agrees quantitatively with the results on in Figure 7. Therefore, based on gasdynamics, the bright feature of transient corresponds to the compressed flow and the shock front ahead of the moving piston, and the darker feature of transient corresponds to the rarefaction flow behind the moving piston. This physical picture agrees with the results given by observations.

6. The Structure of the Moving Plasma Piston

In the above discussion, the piston of moving plasma was treated as a solid plane, and the plasma density on both sides of the piston was determined. In fact, the piston discussed here consists of layers of moving plasma. The prominence plasma has a typical thickness of 10^4 km, which will increase when the eruptive prominence moves and expands outward in the corona. Furthermore, the eruptive prominence often emerges into the solar active region, where the magnetic field is usually stronger and closed. When this occurs, the magnetic field is pulled, and a magnetic flux layer forms ahead of the eruptive prominence. Therefore, the piston of moving plasma may be considered typically to have a structure which consists of at least two layers, the magnetic flux layer (arcade or loop) and the eruptive prominence itself.

There are three boundaries, that it, the interface between the compressed flow and the region of the compressed magnetic field, the interface between the region of the magnetic field and the eruptive prominence, and the interface between the eruptive prominence and the rarefaction flow. According to the frozen condition, there is no mass exchange between the eruptive prominence and the region of the compressed magnetic field or the rarefaction region. Therefore, the boundaries are a tangential discontinuous surface, and we have the relations

$$p_{\mathrm{II}} + \frac{B_{\mathrm{II}}^2}{8\pi} = p_{em} + \frac{B_{em}^2}{8\pi} , \quad \text{at the first interface} \tag{6.1}$$

$$p_{em} + \frac{B_{em}^2}{8\pi} = p_{ep} + \frac{B_{ep}^2}{8\pi} , \quad \text{at the second interface} \tag{6.2}$$

$$p_{ep} + \frac{B_{ep}^2}{8\pi} = p_{\mathrm{III}} + \frac{B_{\mathrm{III}}^2}{8\pi} , \quad \text{at the third interface} \tag{6.3}$$

where the subscription *em* and *ep* correspond to the region of the compressed magnetic field and the eruptive prominence, respectively. As the strength of the magnetic field and the temperature are different in different regions, the density will discontinuous across these interfaces. The magnetic field in the quiet corona is much weaker than the one in

the region of the compressed magnetic field, so we obtain generally

$$p_1 \approx P_{em} + B_{em}^2/8\pi\,, \quad \text{at the first interface}\,. \tag{6.4}$$

This relation shows that the density in the region of compressed magnetic flux just ahead of the eruptive prominence is lower than the density in the quiet corona if the temperature has not changed greatly. Thus, in front of the eruptive prominence, there is a darker region corresponding to the region of compressed magnetic flux. The stronger the magnetic field, the darker will be the region. As discussed in the last section, ahead of this darker region is a bright region which corresponds to the compressed region produced by the moving piston.

The density is high and the temperature is low in the prominence. According to (6.2), the pressure in the prominence will be larger than the pressure p_{em} if the magnetic field is stronger in the region of emerging magnetic flux. The third interface which divides the eruptive prominence and the rarefaction flow is also a tangential discontinuous surface, and the density will jump from a high value in the prominence to a small one in the rarefaction flow across the interface. However, the strength of the discontinuity may decrease because of the effect of expansion in the prominence; that is, the prominence density will be small toward the rarefaction flow. Therefore, the structure of the moving plasma may be treated as having at least two layers. Considering this structure and the results in the last section, the density distribution for a transient process along the z direction is given in Figure 15. This profile agrees qualitatively with observations.

Some theoretical models of coronal transients are based on the concept of an emerging magnetic flux driven by the Lorentz force. The kinetic features, especially the acceleration process, of a transient may be described by this approach. However, the

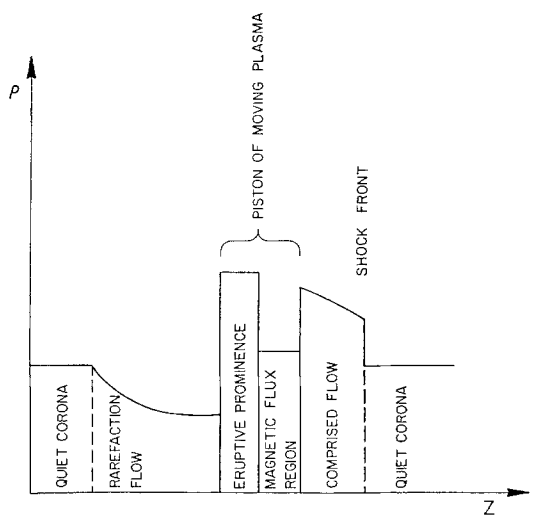

Fig. 15. The structure of the moving plasma piston, consisting of the eruptive prominence and the magnetic flux region.

region of emerging magnetic flux corresponds to the region of lower density as shown in the relation (6.1), and the basic feature of the transient is the propagation of the high-density loop, which is difficult to explain if the gas-dynamical effect in front of the emerging flux is excluded.

The present paper suggests that a coronal transient is driven by a piston of moving plasma, which consists of an eruptive prominence and a magnetic flux region or tube. The gasdynamical effect is the same whether the driving force is the eruptive prominence or the Lorentz force acting on the magnetic flux tube. Furthermore, the Lorentz force in the moving flux tube may be induced by the eruptive prominence. However, it seems preferable to consider that the eruptive prominence may be the driving source of the transient associated with it.

7. Discussion

Observations from space and on the ground are yielding more and more information about coronal transients, especially about their initial process and fine structure. It has become evident that the coronal transient is a complex dynamical process, including both compression and depletion. The purpose of this paper has been to discuss the physical picture and the major mechanism, and to suggest that a piston of moving plasma, consisting of an eruptive prominence and a magnetic flux region, may be the driving force for the transient process. Furthermore, we analyzed the dynamical effects of the moving piston, which produces a compressed region ahead of it and a rarefaction region behind it. On this basis, the bright features and dark features of the transient process may be explained at the same time. Moreover, the dynamical process also sheds light on the fine structure of the transient, which may be compared with observations.

Figure 14 describes clearly the bright feature. The bright transient is located between the piston and the shock front at any particular time; it is nearly constant in case (5.14), and will increase linearly in case (5.13). The width of compressed region depends on the velocity distribution of the piston; however, this width is much smaller than that of the rarefaction region. Therefore, observations will give a configuration with a narrow bright front and a broad dark region behind it. As the strength of the shock wave is weak at the initial period and increases gradually, the bright front is not very clear at the beginning, but as the brightness increases, it becomes clearer. Figure 14 shows also that the velocity of the shock front is also nearly constant, or slightly accelerating. These features agree well with observations.

It will be pointed out that the velocity of the bright transient given in present paper corresponds to the velocity of the shock front, which is different from the velocity of the piston (the magnetic loop or eruptive prominence) itself. Therefore, the acceleration process of the bright transient is associated with formation and propagation of the shock front, instead of the moving piston itself.

Statistical correlations show that there are at least two kinds of transients, one associated with an eruptive prominence and the other associated with a solar flare. We have discussed only the former case. Whether a similar mechanism may be applied to the latter should be studied further.

Appendix I. Characteristic Relationships

The gasdynamical Equations (3.1)–(3.3) may be rewritten as

$$\frac{\gamma-1}{2}\, a\, \frac{\partial w}{\partial z} + \frac{\partial a}{\partial t} + w\, \frac{\partial a}{\partial z} = 0\,, \tag{A.I-1}$$

$$\frac{\partial w}{\partial t} + w\, \frac{\partial w}{\partial z} + \frac{2a}{\gamma-1}\, \frac{\partial a}{\partial z} - \frac{a^2}{\gamma-1}\, \frac{1}{s}\, \frac{\partial s}{\partial z} = -\frac{GM}{z^2}\,, \tag{A.I-2}$$

$$\frac{\partial s}{\partial t} + w\, \frac{\partial s}{\partial z} = 0\,. \tag{A.I-3}$$

where we define

$$s = (p/\rho^{\gamma})^{\gamma} \tag{A.I-4}$$

and the sonic velocity

$$a = \left(\frac{\gamma p}{\rho}\right)^{1/2} \tag{A.I-5}$$

Discussing the initial value problem, we give the distributions of the parameters at the curve

$$z = Z(t) \tag{A.I-6}$$

as

$$w(z, t) = w[Z(t), t]\,, \qquad a(z, t) = a[Z(t), t]\,, \qquad s(z, t) = s[Z(t), t]\,, \tag{A.I-7}$$

so then, we have the relation

$$\frac{\partial}{\partial t} = \frac{\mathrm{d}}{\mathrm{d}t} - Z'(t)\, \frac{\partial}{\partial z}\,. \tag{A.I-8}$$

along curve (A.I-6), and $\mathrm{d}/\mathrm{d}t$ is the differential along the curve. Using the relation (A.I-8), the basic equations (A.I-1)–(A.I-3) reduce to

$$\frac{\gamma-1}{2}\, a\, \frac{\partial w}{\partial z} + (w - z')\, \frac{\partial a}{\partial z} = -\frac{\mathrm{d}a}{\mathrm{d}t}\,, \tag{A.I-9}$$

$$(w - z')\, \frac{\partial w}{\partial z} + \frac{2a}{\gamma-1}\, \frac{\partial a}{\partial z} = \frac{a^2}{\gamma-1}\, \frac{1}{s}\, \frac{1}{z' - w}\, \frac{\mathrm{d}s}{\mathrm{d}t} - \frac{\mathrm{d}w}{\mathrm{d}t} - \frac{GM}{z^2}\,, \tag{A.I-10}$$

$$(w - z')\, \frac{\partial s}{\partial z} = -\frac{\mathrm{d}s}{\mathrm{d}t}\,. \tag{A.I-11}$$

The characteristic line is the line that the flow field near the line cannot be determined if the initial conditions are given at the line. Therefore, relatinships (A.I-9) and (A.I-10) gave first and second characteristic lines and (A.I-11) gives third one. Substituting the characteristic conditions into Equations (A.I-9)–(A.I-11), we obtain the characteristic relationships. These results may be written as follows:

$$z' = w + a\,, \tag{A.I-12}$$

$$\mathrm{d}w + \frac{2}{\gamma - 1}\,\mathrm{d}a = \frac{a}{\gamma - 1}\,\mathrm{d}\ln s - \frac{GM}{z^2}\,\mathrm{d}z\,, \tag{A.I-13}$$

$$Z' = w - a\,, \tag{A.I-14}$$

$$\mathrm{d}w - \frac{2}{\gamma - 1}\,\mathrm{d}a = -\frac{a}{\gamma - 1}\,\mathrm{d}\ln s - \frac{GM}{z^2}\,\mathrm{d}z \tag{A.I-15}$$

and

$$z' = w\,, \tag{A.I-16}$$

$$\mathrm{d}s = 0\,, \tag{A.I-17}$$

The third relations (A.I-16) and (A.I-17) are those of the stream line.

The relationships (A.I-13) and (A.I-15) may be rewritten as

$$(w + a)\left(\mathrm{d}w + \frac{2}{\gamma - 1}\,\mathrm{d}a\right) + \frac{GM\,\mathrm{d}z}{z^2} = \frac{a(w + a)}{\gamma - 1}\,\mathrm{d}s \tag{A.I-18}$$

and

$$(w - a)\left(\mathrm{d}w - \frac{2}{\gamma - 1}\,\mathrm{d}a\right) + \frac{GM\,\mathrm{d}z}{z^2} = -\frac{a(w - a)}{\gamma - 1}\,\mathrm{d}s \tag{A.I-19}$$

respectively. The terms in the right-hand side of both equations are zero if the entropy remains constant everywhere.

Appendix II. The Characteristic Relations of Finite Difference

If the velocity of a piston is given, the trajectory of the piston is a given curve in plane (z, t), which may be written as

$$z^* = z^*(t^*)\,. \tag{A.II-1}$$

If the sonic velocity is also given at curve (A.II-1), the characteristic lines and the flow field near the trajectory (A.II-1) may be calculated. For two near points $A_0(z_0^*, t_0^*)$ and $A_1(z_1^*, t_1^*)$ at curve (A.II-1), the characteristic line (5.1) passing A_0 crosses the characteristic line (5.2) passing A_1 at point $A_2(z_2^*, t_2^*)$ as shown in Figure 16. The

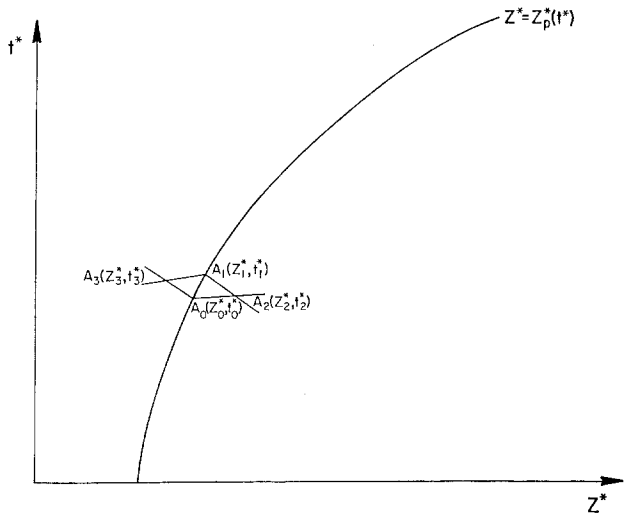

Fig. 16. Schematic diagram of the finite differences between characteristic lines and relationships.

position of A_2 may be determined by (5.1) and (5.3) as

$$t_2^* = \frac{(w_0^* + a_0^*)t_0^* - (w^* - a_1^*)t_1^* + (z_1^* - z_0^*)}{(w_0^* + a_0^*) - (w_1^* - a_1^*)}, \tag{A.II-2}$$

$$z_2^* = \frac{z_1^*(w_0^* + a_0^*) - z_0^*(w_1^* - a_1^*) + (w_0^* + a_0^*)(t_0^* - t_1^*)(w_1^* - a_1^*)}{(w_0^* + a_0^*) - (w_1^* - a_1^*)}. \tag{A.II-3}$$

For the characteristic relationships (5.2) and (5.4), the parameters of the flow field at A_2 are

$$w_2^* = -\frac{1}{2}\left(\frac{\Delta t_{20}^*}{z_{20}^{*2}} + \frac{\Delta t_{21}^*}{z_{21}^{*2}}\right) + \left(\frac{w_0^*}{2} + \frac{a_0^*}{\gamma - 1}\right) + \left(\frac{w_1^*}{2} - \frac{a_1^{*2}}{\gamma - 1}\right), \tag{A.II-4}$$

$$a_2^* = \frac{\gamma - 1}{4}\left(\frac{\Delta t_{20}^*}{z_{20}^{*2}} + \frac{\Delta t_{21}^*}{z_{21}^{*2}}\right) + \frac{\gamma - 1}{2}\left(\frac{w_0^*}{2} + \frac{a_0^*}{\gamma - 1}\right) - \frac{\gamma - 1}{2}\left(\frac{w_1^*}{2} - \frac{a_1^*}{\gamma - 1}\right) \tag{A.II-5}$$

where

$$\Delta t_{20}^* = t_2^* - t_0^*, \qquad \Delta t_{21}^* = t_2^* - t_1^*,$$

$$z_{20}^* = \tfrac{1}{2}(z_2^* + z_0^*), \qquad z_{21}^* = \tfrac{1}{2}(z_2^* + z_1^*).$$

Step by step, the above relations give the flow field to the right of the trajectory of the piston, which region corresponds to the compressed flow.

Similarly, the flow field to the left of the piston trajectory may also be given. For the crossed point $A_3(z_3^*, t_3^*)$ as shown in Figure 16, we have

$$t_3^* = \frac{z_0^* - z_1^* + (w_1^* + a_1^*)t_1^* - (w_0^* - a_0^*)t_0^*}{(w_1^* + a_1^*) - (w_0^* - a_0^*)} \tag{A.II-6}$$

$$z_3^* = \frac{z_0^*(w_1^* + a_1^*) - z_1^*(w_0^* - a_0^*) + (w_1^* + a_1^*)(w_0^* - a_0^*)(t_1^* - t_0^*)}{(w_1^* + a_1^*) - (w_0^* - a_0^*)} \tag{A.II-7}$$

and

$$a_3^* = -\frac{\gamma - 1}{4}\left(\frac{\Delta t_{30}^*}{z_{30}^{*2}} + \frac{\Delta t_{31}^*}{z_{31}^{*2}}\right) + \left(\frac{a_0^*}{2} - \frac{\gamma - 1}{4} w_0^*\right) + \left(\frac{a_1^*}{2} + \frac{\gamma - 1}{4} w_1^*\right), \tag{A.II-8}$$

$$w_3^* = -\frac{1}{2}\left(\frac{\Delta t_{30}^*}{z_{30}^{*2}} + \frac{\Delta t_{31}^*}{z_{31}^{*2}}\right) + \left(\frac{w_0^*}{2} - \frac{a_0^*}{\gamma - 1}\right) + \left(\frac{w_1^*}{2} + \frac{a_1^*}{\gamma - 1}\right), \tag{A.II-9}$$

where

$$\Delta t_{30}^* = t_3^* - t_0^*, \qquad \Delta t_{31}^* = t_3^* - t_1^*,$$

$$z_{30}^* = \tfrac{1}{2}(z_3^* + z_0^*), \qquad z_{31}^* = \tfrac{1}{2}(z_3^* + z_1^*).$$

References

Allen, C. W.: 1973, *Astrophysical Quantities*, Athlone Press, Univ. of London.
Anzer, U.: 1978, *Solar Phys.* **57**, 111.
Chipman, E. G.: 1981, *Astrophys. J.* **244**, L113.
Dryer, M.: 1981, *Solar Wind Four*, Rep. No. MPAE–W–100–81–31.
Dryer, M., Wu, S. T., Stienolfson, R. S., and Wilson, R. M.: 1979, *Astrophys. J.* **227**, 1059.
Fisher, R. and Poland, A. I.: 1981, *Astrophys. J.* **246**, 1004.
Howard, R. A. *et al.*: 1976, NOAA World Data Center A, UAG-48A.
Landau, L. D. and Lifshitz, E. M.: 1959, *Fluid Mechanics*, Pergamon Press, Oxford.
Low, B. C.: 1982, *Astrophys. J.* **254**, 335.
Low, B. C., Munro, R. H., and Fisher, R.: 1982, *Astrophys. J.* **246**, 1004.
MacQueen, R. M.: 1980, *Phil. Trans. Roy. Soc. London* **A297**, 605.
MacQueen, R. M., Eddy, J. A., Gosling, J. T., Hildner, E., Munro, R. H., Newkirk, G. A., Poland, A. I., and Ross, C. L.: 1974, *Astrophys. J.* **187**, L85.
Maxwell, A. and Dryer, M.: 1981, *Solar Phys.* **73**, 313.
Mouschovias, T. C. and Poland, A. I.: 1978, *Astrophys. J.* **220**, 675.
Munro, R. H., Gosling, J. T., Hildner, E., MacQueen, R. M., Poland, A. I., and Ross, C. L.: 1979, *Solar Phys.* **61**, 201.
Nakagawa, Y., Wu, S. T., and Tandberg-Hanssen, E.: 1975, *Solar Phys.* **41**, 387.
Nakagawa, Y., Wu, S. T., and Han, S. M.: 1978, *Astrophys. J.* **219**, 314.
Pneuman, G. W.: 1980, *Solar Phys.* **65**, 369.

Rust, D. M., Hildner, E., Dryer, M., Hanson, R. T., McClymont, A. N., McKenna-Lawler, S. M. P., McLean, D. J., Schmahl, E., Steinolfson, R. S., Tandberg-Hanssen, E., Tousey, R., Webb, D., and Wu, S. T.: 1979, in P. Sturrock (ed.), *Solar Flares*, p. 273.
Sedov, L. I.: 1959, *Similarity and Dimensional Methods in Mechanics*, Academic Press.
Stanyukovich, K. P.: 1960, *Unsteady Motion of Continuous Media*, Pergamon Press, Oxford.
Steinolfson, R. S. and Nakagawa, Y.: 1977, *Astrophys. J.* **215**, 345.
Tandberg-Hanssen, E.: 1974, *Solar Prominences*, D. Reidel Publ. Co., Dordrecht, Holland.
Thompson, P. A.: 1972, *Compressible-Fluid Dynamics*, McGraw-Hill Book Co., New York, Chapter 8.
Wu, S. T., Dryer, M., Nakagawa, Y., and Han, S. M.: 1978, *Astrophys. J.* **219**, 324.
Yeh, T. and Dryer, M.: 1981, *Astrophys. J.* **245**, 704.